Isocyanide and Diisocyanide Complexes of a Triplatinum Cluster: Fluxionality, Isomerism, Structure, and Bonding

Arleen M. Bradford, Eva Kristof, Mehdi Rashidi, Dong-Sheng Yang, Nicholas C. Payne, and Richard J. Puddephatt*

Department of Chemistry, The University of Western Ontario, London, Canada N6A 5B7

Received July 28, 1993®

The reaction $[Pt_3(\mu_3\text{-}CO)(\mu\text{-}dppm)_3]^{2+}$, **1**, with RNC (R = *t*-Bu, cyclohexyl or *o*-xylyl) gives an intermediate characterized as $[Pt_3(\mu\text{-}CO)(CNR)(\mu\text{-}dppm)_3]^{2+}$, **2**, which then isomerizes to the stable complex $[Pt_3(\mu_3\text{-}CO)(CNR)(\mu\text{-}dppm)_3]^{2+}$, **3**. When R = *o*-xylyl, reaction of **3** with more RNC gives an intermediate $[Pt_3(\mu\text{-}CO)(CNR)_2(\mu\text{-}dppm)_3]^{2+}$, **4**, which then loses CO to give $[Pt_3(CNR)_2(\mu\text{-}dppm)_3]^{2+}$, **5**, the first example of a Pt_3 cluster complex having no bridging atom. The cluster **5** has been characterized by an X-ray structure determination. [The solvated salt crystallizes in the monoclinic space group $P2_1$, cell dimensions a = 17.639(2) Å, b = 19.704(3) Å, c = 14.5444(12) Å, and β = 101.99(2)° with Z = 2. Full matrix least-squares refinement on F^2 of 558 variables converged at a conventional R factor of 0.0393 for 6334 data with $I > 2\sigma(I)$.] The two xylyl isocyanide ligands are *trans*-bonded to Pt(1), and as a result the Pt(2)–Pt(3) distance of 2.548(1) Å is significantly shorter than the mean of the two distances to Pt(1), 2.649(1) Å. Complexes **3** and **5** are fluxional; the RNC ligands can migrate easily around the face of the Pt_3 triangle. The diisocyanides 1,4-C≡NC_6R_4N≡C, R = H or Me, react with **1** to give polymeric complexes $\{[Pt_3(\mu\text{-}1,4\text{-}C{\equiv}NC_6R_4N{\equiv}C)(\mu\text{-}dppm)_3][PF_6]_2\}_n$, **7**, in which the diisocyanide bridges between Pt_3 cluster units. The local stereochemistry at platinum is similar to that in **5**, and the fluxionality appears even easier in **7** than in **5**. Evidence is presented for diisocyanide complexes analogous to **2** and **3**, namely $[Pt_3(\mu\text{-}CO)(CNC_6H_4NC)(\mu\text{-}dppm)_3]^{2+}$ and $[\{Pt_3(\mu_3\text{-}CO)(\mu\text{-}dppm)_3\}_2(\mu\text{-}CNC_6H_4NC)]^{4+}$, **8**. Calculations of the EHMO type on model complexes give insight into the factors which influence the preferred binding mode (terminal or triply bridging) of the isocyanide at the Pt_3 triangle.

Introduction

The complex cation $[Pt_3(\mu_3\text{-}CO)(\mu\text{-}dppm)_3]^{2+}$, **1**, dppm = $Ph_2PCH_2PPh_2$, is a coordinatively unsaturated cluster with each platinum atom having a vacant $6p_z$ orbital.[1] Since the $Pt_3(\mu\text{-}dppm)_3$ unit in **1** is approximately planar, access of additional ligands to the Pt_3 triangle must occur initially from above or below the Pt_3 plane, and since the $Pt_3(\mu\text{-}dppm)_3$ unit is not easily broken, these ligand adducts can often be isolated.[2] This combination of properties makes the cluster **1** a useful mimic of the chemical properties of a Pt_3 unit of a platinum surface, in which one can consider the Pt_3 triangle to be locked in place by the surrounding matrix of platinum atoms. Ligands can bind to a Pt(111) surface at terminal (on-top), doubly bridging (2-fold), or triply bridging (3-fold) sites, and the easy movement of ligands between such sites leads to fluxionality or ligand mobility; similar bonding modes and fluxionality are also possible when ligands add to complex **1**.[2]

This paper reports the interaction of isocyanide ligands (RNC with R = *t*-Bu, cyclohexyl, or *o*-xylyl) with the cluster **1**. The ligand MeNC [ν(NC) = 2190 cm^{-1}] binds to a platinum(111) surface in either terminal, **A** [ν(NC) = 2265–2240 cm^{-1}], or

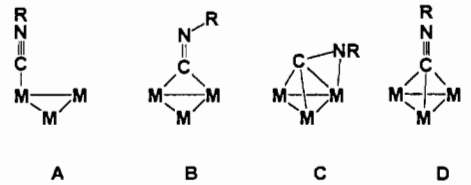

A B C D

doubly bridging, **B** [ν(NC) = 1600–1770 cm^{-1}], bonding modes with the frequency and relative amounts of **A** and **B** depending on the surface coverage.[3] These same bonding modes are found in several platinum cluster complexes with isocyanide ligands.[4] On a nickel(111) surface, MeNC may bind as a μ_3-η^2-ligand, **C**,[5] while in Ni_3 clusters it may bind in forms **A**, **B**, or **D**.[6] The major interest is in how the isocyanide ligands bind to the Pt_3 triangle of **1** and in the easy fluxionality of the isocyanide ligands in the product clusters. A preliminary account of parts of this work has been published, as well as an account of related chemistry with methyl isocyanide; much of the chemistry with MeNC is similar to that described below, but there are also significant differences.[7,8]

Finally, the reactions of diisocyanides with **1** have been studied, and evidence for the formation of the first polymers with the diisocyanides bridging between Pt_3 clusters is reported.

Results

Reactions with 1 equiv of RNC. The results are shown in eq 1.

* Abstract published in *Advance ACS Abstracts,* May 1, 1994.

(1) Ferguson, G.; Lloyd, B. R.; Puddephatt, R. J. *Organometallics* **1986**, *5*, 344.
(2) Puddephatt, R. J.; Manojlovic-Muir, Lj.; Muir, K. W. *Polyhedron* **1990**, *9*, 2767.
(3) (a) Avery, N. R.; Matheson, T. W. *Surf. Sci.* **1984**, *143*, 110. (b) Szilagyi, T. *Appl. Surf. Sci.* **1988**, *35*, 19.
(4) (a) Green, M.; Howard, J. A.; Spencer, J. L.; Stone, F. G. A. *J. Chem. Soc., Chem. Commun.* **1975**, 3. (b) Yamamoto, Y.; Takahashi, K.; Yamazaki, H. *Chem. Lett.* **1985**, 201. (c) Yamamoto, Y.; Takahashi, K.; Yamazaki, H. *J. Am. Chem. Soc.* **1986**, *108*, 2458. (d) Briant, C. E.; Gilmour, D. I.; Mingos, D. M. P. *J. Organomet. Chem.* **1986**, *308*, 381. (e) Mingos, D. M. P.; Williams, I. D.; Watson, M. J. *J. Chem. Soc., Dalton Trans.* **1988**, 1509. (f) Mingos, D. M. P.; Slee, T. *J. Organomet. Chem.* **1990**, *394*, 679. (g) Briant, C. E.; Gilmour, D. E.; Mingos, D. M. P.; Wardle, R. W. M. *J. Chem. Soc., Dalton Trans.* **1985**, 1693.
(5) Muetterties, E. L.; Bard, E.; Kokorin, A.; Pretzer, W. R.; Thomas, M. G. *Inorg. Chem.* **1980**, *19*, 1377.
(6) (a) Ratliff, K. S.; Broeker, G. K.; Fanwick, P. E.; Kubiak, C. P. *Angew. Chem., Int. Ed. Engl.* **1990**, *29*, 395. (b) Ratliff, K. S.; Fanwick, P. E.; Kubiak, C. P. *Polyhedron* **1990**, *9*, 1487. (c) Kristof, E.; Rashidi, M.; Vittal, J. J.; Puddephatt, R. J. *Inorg. Chem.*, submitted for publication.
(7) Bradford, A. M.; Payne, N. C.; Puddephatt, R. J.; Yang, D.-S.; Marder, T. B. *J. Chem. Soc., Chem. Commun.* **1990**, 1462.
(8) Puddephatt, R. J.; Rashidi, M.; Vittal, J. J. *J. Chem. Soc., Dalton Trans.* **1991**, 2835.

0020-1669/94/1333-2355$04.50/0

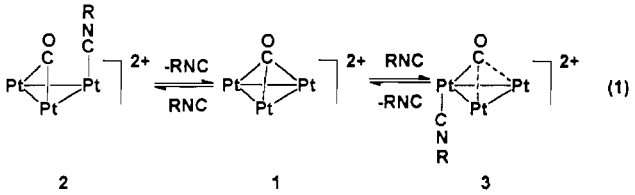

2 1 3

The complexes **2** (**2a**, R = *t*-Bu; **2b**, R = Cy = cyclohexyl) were formed only at low temperatures and could not be isolated. They were characterized by low-temperature NMR spectroscopy (Table 1 and Experimental Section). In contrast, the complexes **3** (**3a**, R = *t*-Bu; **3b**, R = Cy; **3c**, R = Xy = *o*-xylyl = 2,6-$Me_2C_6H_3$) were stable compounds and could be isolated as red solid compounds with PF_6^- counterions.

The complex **3b**$[PF_6]_2 \cdot Me_2CO$ was characterized crystallographically, but unfortunately, severe disorder involving the carbonyl and isocyanide ligands prevented the accurate location of these ligands.[9] The Pt–Pt distances were Pt(1)–Pt(2) = 2.646(3), Pt(2)–Pt(3) = 2.626(3), and Pt(2)–Pt(3) = 2.585(3) Å, and both carbonyl and isocyanide ligands were bound primarily to Pt(1). Further characterization was possible using IR and NMR spectroscopies.

The IR spectra for each complex **3** contained two bands in the region 1700–2200 cm^{-1}. The band at 2131–2170 cm^{-1} is assigned to ν(C≡N) of the isocyanide ligand and clearly indicates a terminal bonding mode for this ligand. The band at 1780–1800 cm^{-1} is due to ν(CO), and this assignment was confirmed by recording the spectra of ^{13}CO-labeled derivatives. For comparison, complex **1** has ν(CO) = 1765 cm^{-1}. The ν(CO) values are clearly too low for a terminal carbonyl. For a symmetrical ν_3-CO ligand, a lower stretching frequency might be expected for **3** than for **1** since stronger back-bonding to CO should occur on coordination of the RNC ligand. The ν(CO) stretching frequencies for **3** are slightly higher than for **1**, and this is consistent with a structure with an unsymmetrical (or semibridging) μ_3-CO ligand as shown in structure **3** (Chart 1).

Since the complexes were fluxional at room temperature, they were characterized by multinuclear NMR spectroscopy at −80 °C in acetone-d_6. The ^{31}P NMR spectra each contained three resonances due to P^a, P^b, and P^c (see structure **3** in Chart 1 for NMR labeling scheme), and the long-range coupling $^3J(P^aP^c)$ and $^3J(P^bP^{b'})$ of 160–200 Hz are typical of such couplings through a metal–metal bond.[10] The ^{13}C NMR spectra were obtained on the ^{13}CO substituted derivatives **3***. Each complex **3*** gave a 1:4:1 triplet, due to the coupling $^1J(Pt^1C)$ = 1175–1200 Hz, of 1:8:18:8:1 quintets, due to the couplings $^1J(Pt^2C) = {}^1J(Pt^3C)$ = 400–458 Hz. A typical spectrum is shown in Figure 1a. The much larger coupling $^1J(Pt^1C)$ clearly indicates that the carbonyl is bound most strongly to this platinum atom. In the room-temperature spectrum, Figure 1b, an "average" PtC coupling is observed. The ^{195}Pt NMR spectrum of **3** (Figure 2) contained a triplet due to Pt^1 and a doublet of doublets due to Pt^2, as a result of ^1J(PtP) couplings. In the spectra of **3***, an additional coupling due to ^1J(PtC) was observed for each resonance (Figure 3). Correlation of these couplings ^1J(PtP) and ^1J(PtC) from the ^{13}C, ^{31}P, and ^{195}Pt NMR spectra was a major aid in making positive assignments. For complex **3a** (Figure 2), the Pt^1 resonance was clearly resolved as a 1:2:1 triplet of 1:8:18:8:1 quintets, the latter arising from the coupling $^1J(Pt^1Pt^2)$ = 750 Hz, but this PtPt coupling was not resolved in all cases.[10] The ^{195}Pt signals could not be detected in room-temperature spectra, presumably because dynamic effects led to extreme broadening of the resonances.[10]

When 1 equiv of *t*-BuNC or CyNC was added to a solution of **1** at −80 °C and NMR spectra recorded at this temperature, the complexes **2** were formed as the sole or major product (complex **3** was also present in some cases). As the solutions were warmed to room temperature slow conversion to **3** occurred, but cooling solutions of **3** to −80 °C did not cause formation of **2**. The complexes **2** were not fluxional over the temperature range where they could be detected. Thus, for example, the ^{31}P NMR spectrum of a solution containing both **2b** and **3b** at −22 °C contained sharp resonances due to **2b** but the resonances due to **3b** were broad due to the onset of fluxionality of this complex.

The ^{31}P NMR spectra of **2** contained three resonances assigned to P^a, P^b, and P^c and, as usual, the large values of $^3J(P^aP^c)$ and $^3J(P^bP^{b'})$ indicate couplings through PtPt bonds. Three ^{31}P resonances are observed for $Pt_3(\mu\text{-dppm})_3$ clusters when there is one plane of symmetry perpendicular to the Pt_3 plane.[10] All resonances exhibit ^1J(PtP) coupling proving that no displacement of dppm has occurred (Table 1). The ^{13}C NMR spectra of ^{13}CO labeled derivatives **2*** each gave a single resonance, which appeared as a 1:8:18:8:1 quintet due to ^1J(PtC) coupling, thus proving the presence of a $Pt_2(\mu_2\text{-CO})$ group. No coupling to the third platinum center or to phosphorus was resolved. The solubilities of **2** at low temperature were too low to allow satisfactory ^{195}Pt NMR spectra to be obtained.

The above spectroscopic data do not distinguish between the structures **2** and **2′**, but given the ease of migration of ligands about the Pt_3 face, it would be expected that **2′** would very easily convert to **3**. On the other hand, **2** has both CO and RNC ligands on the same side of the Pt_3 plane and hence rearrangement to **3** must occur by dissociation of one ligand (probably RNC) followed by recoordination to the opposite face. Study of space-filling models shows that neither **2** nor **2′** is sterically forbidden. It is not clear why **2** is formed at low temperature, but it is presumably a kinetic effect. One possibility is that the conformation of the

Table 1. Selected ^{31}P and ^{195}Pt NMR Data for the Clusters **2–5**

complex	$\delta(P^a)$	$\delta(P^b)$	$\delta(P^c)$	$\delta(Pt^1)$	$\delta(Pt^2)$	$^1J(PtP^a)$	$^1J(PtP^b)$	$^1J(PtP^c)$
2a	−32.5	−55.8	−23.4			2120	3030	3400
2b	−33.2	−53.9	−18.7			2220	3180	3240
2d	−37.45	−47.15	−14.9			2200	3300	3372
3a	−43.1	−3.1	−6.7	−3247	−2132	1850	2510	4030
3b	−45.7	−4.1	−6.7	−3234	−2141	1850	2550	4040
3c	−38.9	−3.0	−2.8	−3269	−2493	2680	3200	4020
4	−34.8	−56.5	−17.7			2200	3090	3380
5	−41.4	−1.3	−10.7	−3190	−2002	1760	2440	4030

Chart 1. NMR Labeling

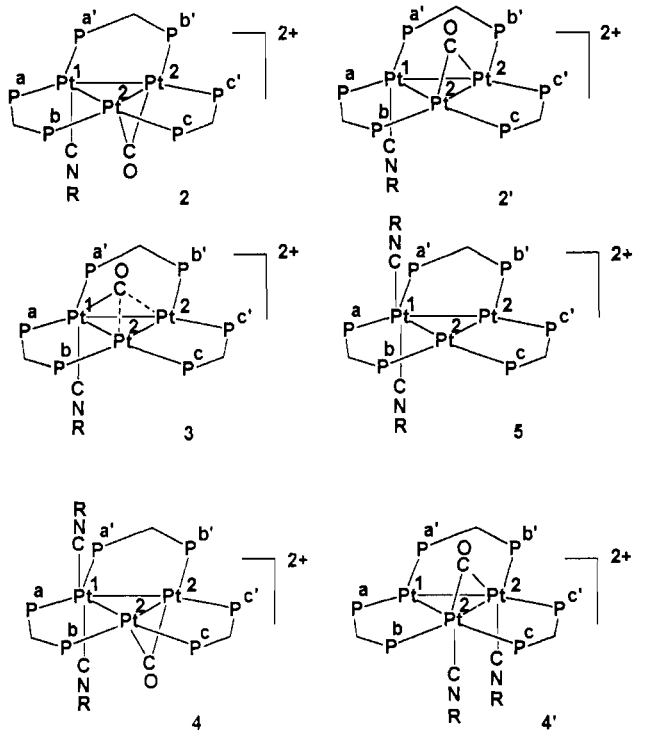

2 2′ 3 5 4 4′

(9) Manojlovic-Muir, Lj.; Muir, K. W. Unpublished work.
(10) (a) Bradford, A. M.; Douglas, G.; Manojlovic-Muir, Lj.; Muir, K. W.; Puddephatt, R. J. *Organometallics* **1990**, *9*, 409. (b) Moor, A.; Pregosin, P. S.; Venanzi, L. M. *Inorg. Chim. Acta* **1982**, *61*, 135. (c) Pregosin, P. S. *Coord. Chem. Rev.* **1982**, *44*, 247.

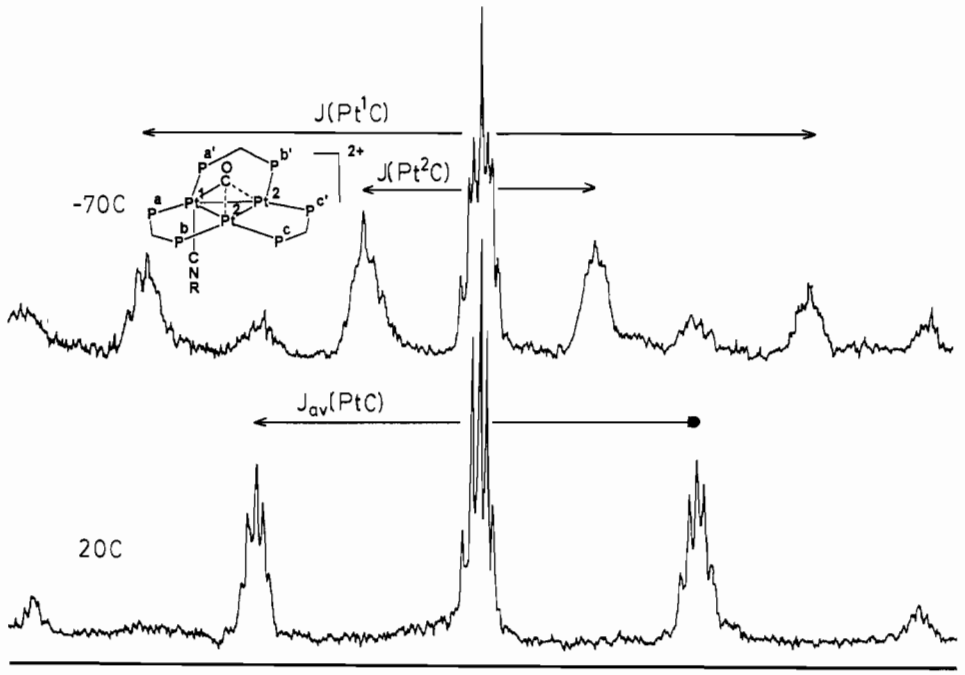

Figure 1. ^{13}C NMR spectra of complex **3a**: (a, top) spectrum at −70 °C, with the separate PtC couplings indicated; (b, bottom) spectrum at 60 °C, with the "average" PtC coupling indicated. The "average" PtC coupling is expected to be $^1/_3[^1J(Pt^1C) + {}^2/_3[^1J(Pt^2C)] = 700$ Hz which may be compared to the observed value of 688 Hz. The breadth of the peaks in the upper spectrum is probably due to slow dynamic processes.

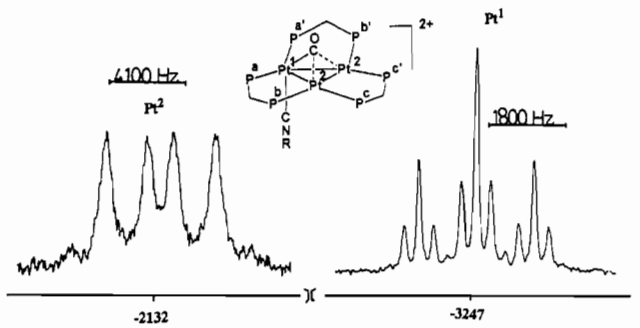

Figure 2. ^{195}Pt NMR spectrum of complex **3a** at −80 °C. Note that the Pt^1 and Pt^2 resonances are recorded at different sweep widths. The breadth of the ^{195}Pt signals is particularly sensitive to residual dynamic effects (compare with sharper lines in Figure 3).

dppm ligands in **1** is such that there is a larger cavity between the phenyl substituents on the carbonyl-bridged face of the Pt_3 triangle than on the opposite face,[1,2] and hence it may be easier for the isocyanide ligand to approach this face and hence form **2** rather than **3**. The weak point of this argument is that the barrier to rearrangement of the envelope conformations of the dppm ligands is low and so the cavity sizes are not fixed, but the effect may still be great enough to give the observed selectivity at −80 °C.

Reaction with 2 mol of Isocyanide. Reaction of complex **3c** with a second equivalent of XyNC gave complex **5**, which could be isolated as the PF_6^- salt in the form of red crystals. Again an intermediate **4** could be detected by low-temperature NMR spectroscopy (eq 2).

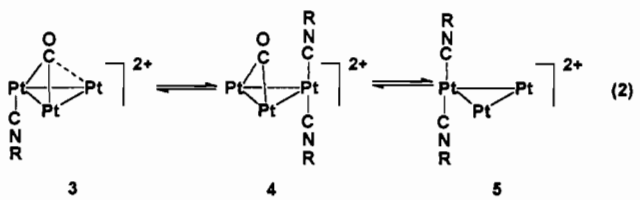

Complex **5** is fluxional, and it was characterized in solution by low-temperature NMR and in the solid state by IR and by an X-ray structure determination. The IR spectrum of **5** contained only one band at 2122 cm^{-1} in the region 1700–2200 cm^{-1} and

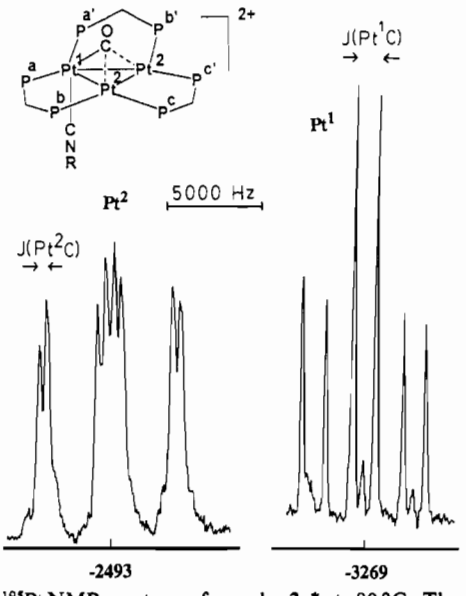

Figure 3. ^{195}Pt NMR spectrum of complex **3c*** at −80 °C. The additional splittings due to $^1J(PtC)$ coupling are indicated. Other splittings are due to $^1J(PtP)$ couplings [note that the coupling $^1J(Pt^1Pt^2)$ is not resolved in this complex].

hence indicates that both isocyanide ligands are terminal. The structure of the cation **5** is shown in Figure 4, and selected bond distances and angles are in Table 2. The crystals are built up from discrete complex cations, PF_6^- anions, and acetone and pentane molecules of solvation, for the shortest nonbonding distance is 2.20 Å between H(5) and H(8B) at $1-x, +y, -z$. The three Pt atoms form an isosceles triangle, the edges of which are bridged by dppm ligands. The Pt atoms and the P atoms of the dppm ligands are roughly coplanar, Table S3 and Figure 5, and the two xylyl isocyanide ligands are *trans*-bonded to Pt(1) at the apex of the triangle. The Pt(2)–Pt(3) distance of 2.584(1) Å is significantly shorter (46σ) than the mean of the two distances to Pt(1), 2.649(1) Å. The Pt(1)–P bonds are also longer than the Pt(2)–P and Pt(3)–P bonds. Hence, there is a general pattern that Pt(1) has the higher coordination number and its bonds to both phosphorus and the other platinum atoms are longer.

The two Pt(1)–C distances are identical, 1.971(2) and 1.972(2) Å. The isocyanide ligands deviate slightly from linearity,

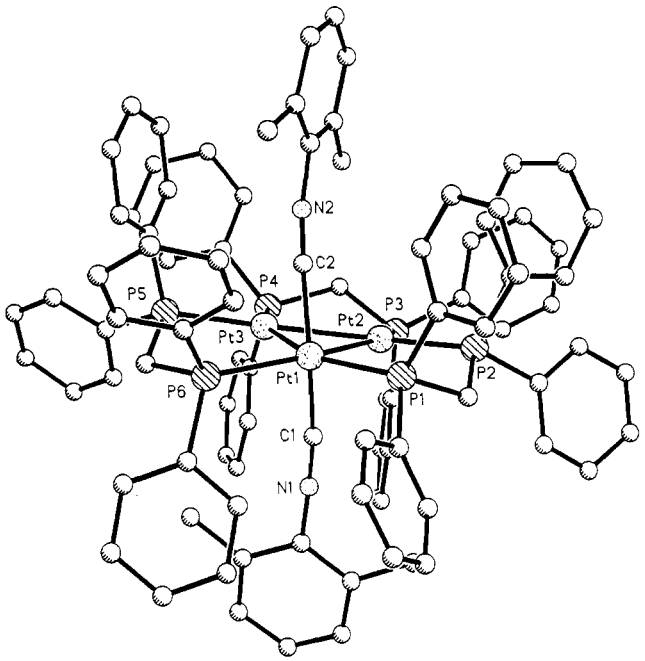

Figure 4. View of the $[Pt_3(\mu\text{-dppm})_3\{C{\equiv}NC_6H_3(CH_3)_2\}_2]^{2+}$ cluster cation.

Table 2. Selected Bond Lengths (Å) and Angles (deg) for **5**

Pt(1)–C(2)	1.97(2)	Pt(1)–C(1)	1.97(2)
Pt(1)–P(6)	2.417(4)	Pt(1)–P(1)	2.420(4)
Pt(1)–Pt(3)	2.6481(9)	Pt(1)–Pt(2)	2.6514(9)
Pt(2)–P(3)	2.219(4)	Pt(2)–P(2)	2.289(4)
Pt(2)–Pt(3)	2.5842(9)	Pt(3)–P(4)	2.237(4)
Pt(3)–P(5)	2.303(5)	P(1)–C(11)	1.825(13)
P(1)–C(3)	1.84(2)	P(1)–C(12)	1.843(13)
P(2)–C(3)	1.82(2)	P(2)–C(14)	1.832(14)
P(2)–C(13)	1.836(14)	P(3)–C(15)	1.819(14)
P(3)–C(16)	1.837(14)	P(3)–C(4)	1.86(2)
P(4)–C(4)	1.81(2)	P(4)–C(18)	1.838(14)
P(4)–C(17)	1.845(14)	P(5)–C(2)	1.812(13)
P(5)–C(110)	1.820(14)	P(5)–C(5)	1.85(2)
P(6)–C(111)	1.810(13)	P(6)–C(5)	1.83(2)
P(6)–C(112)	1.834(13)	C(1)–N(1)	1.16(2)
C(2)–N(2)	1.16(2)	N(1)–C(113)	1.39(2)
N(2)–C(114)	1.39(2)		
C(2)–Pt(1)–C(1)	151.4(6)	C(2)–Pt(1)–P(6)	96.5(6)
C(1)–Pt(1)–P(6)	94.4(5)	C(2)–Pt(1)–P(1)	104.0(5)
C(1)–Pt(1)–P(1)	95.9(4)	C(2)–Pt(1)–Pt(3)	72.9(4)
C(1)–Pt(1)–Pt(3)	79.8(4)	C(2)–Pt(1)–Pt(2)	83.9(5)
C(1)–Pt(1)–Pt(2)	74.6(4)	Pt(3)–Pt(1)–Pt(2)	58.37(2)
Pt(3)–Pt(2)–Pt(1)	60.75(2)	Pt(2)–Pt(3)–Pt(1)	60.88(2)
P(2)–C(3)–P(1)	115.2(8)	P(4)–C(4)–P(3)	109.9(9)
P(6)–C(5)–P(5)	118.5(9)	N(1)–C(1)–Pt(1)	169.0(14)
J(2)–C(2)–Pt(1)	172.8(13)	C(1)–N(1)–C(113)	174(2)
C(2)–N(2)–C(114)	170(2)		

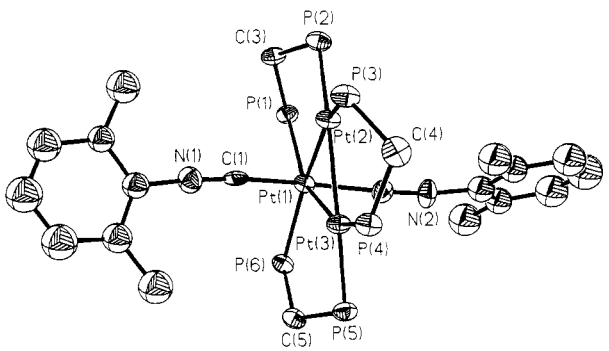

Figure 5. Xylyl ligands and inner cluster cation geometry.

with angles at C of 169(1) and 173(1)° and at N of 170(2) and 174(1)°, Figure 5. The angle C(1)–Pt(1)–C(2) of 151.4(6)° is considerably lower than expected for the limiting *trans*-bonded

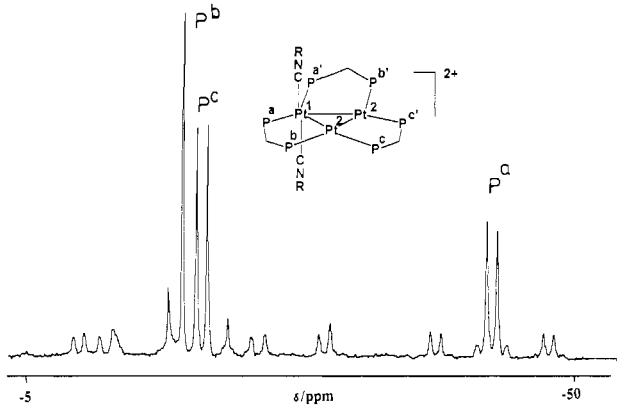

Figure 6. ^{31}P NMR spectrum of complex **5** at −80 °C.

structure of 180°; possible reasons for this will be discussed later. All other dimensions within the cluster cation are in accord with related structures.[1,2,8]

The ^{31}P NMR spectrum of **5** (Figure 6) contained three resonances, and the interpretation is similar to that given for **3c**. In the ^{195}Pt spectrum, the coupling $^1J(Pt^1Pt^2)$ was resolved for **5** but not for **3c**. It is not understood why this coupling is sometimes observed (**3b** and **5**) and sometimes not observed (**3a,c**). The ^1H NMR spectrum gave a single resonance for the methyl protons of the xylyl group and, since the ground-state structure has nonequivalent methyl groups,[7] indicates that rapid rotation about the Pt^1–CNR bond can occur even at −90 °C, the lowest temperature studied.

The intermediate **4** also gave three resonances in the ^{31}P NMR spectrum, indicating the presence of a plane of symmetry perpendicular to the Pt_3 plane. The ^{13}C NMR spectrum contained a single resonance, with a 1:8:18:8:1 appearance due to $^1J(PtC)$ = 908 Hz, thus indicating a doubly bridging carbonyl ligand. The complex **4** was not fluxional up to −20 °C by which temperature complete conversion to **5** and free CO occurred. There are two structures **4** and **4′** which are consistent with the above data. Complex **4′**, with two bulky isocyanides on the same face of the Pt_3 triangle, would be very sterically hindered, and so structure **4** is considered more probable. However, we note that **4′** is analogous to the complexes $[Pt_3(\mu\text{-CO})(CO)_2(\mu\text{-dppm})_3]^{2+}$ and $[Pt_3(\mu\text{-CO})(\mu\text{-}S_2CNR_2)(\mu\text{-dppm})_3]^{+}$ [11] and so cannot be dismissed.

Fluxionality of Complexes 3 and 5. The proposed mechanisms of fluxionality of **3** and **5** are shown in eq 3 and 4. For complexes

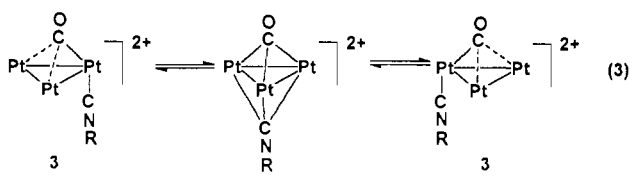

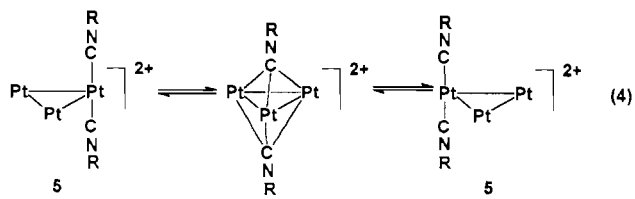

3, the NMR data (Figure 1) show that the CO ligand remains bonded to the cluster during the fluxional process, since the $^1J(PtC)$ coupling is retained, but there is no direct proof that the isocyanide ligand does not dissociate reversibly. However a dissociative mechanism is unlikely to occur so easily and the

(11) (a) Bradford, A. M.; Puddephatt, R. J.; Douglas, G.; Manojlovic-Muir, Lj.; Muir, K. W. *Organometallics* **1990**, *9*, 1579. (b) Lloyd, B. R.; Bradford, A. M.; Puddephatt, R. J. *Organometallics* **1987**, *6*, 424.

proposed mechanism involving reversible formation of a transition state or intermediate with the μ_3-CNR ligand is considered much more probable. The isolation of a 48-electron nickel complex $[Ni_3(\mu_3\text{-CNMe})(\mu_3\text{-I})(\mu\text{-dppm})_3]^+$ and a 42-electron palladium complex $[Pd_3(\mu_3\text{-CNXy})(\mu\text{-dppm})_3]^{2+}$, in which the isocyanide is bridging in the ground state, gives support to the mechanism of eq 4.[6] However, it should be clear that a mechanism in which the isocyanide ligand migrates around the Pt_3 triangle by moving between terminal and edge-bridging bonding modes is not excluded by the NMR data.

For complex **5**, there is no direct spectroscopic evidence that isocyanide ligands remain bonded to the cluster during fluxionality since ^1J(PtC) coupling cannot be detected. Indeed, ^{13}C resonances of the isocyanide ligands were never resolved in any of the isocyanide complexes; clearly ^{13}C enrichment would be necessary for this approach to be successful. However complex **5** does not react with excess XyNC ligand (in contrast to the case with MeNC[8]) and the ^{1}H NMR spectrum of a mixture of **5** and free XyNC at room temperature contained separate resonances for free and coordinated XyNC. Hence, the fluxional process cannot involve reversible dissociation of XyNC and a transition state or intermediate with μ_3-CNR ligands is again most probable.

Fluxionality of isocyanide ligands is unusual, and the ease of the process for **3** and **5** is a further indication of the remarkable properties of coordinatively unsaturated clusers of the group 10 elements. The recent crystallographic characterization of a complex containing a $Pd_3(\mu_3\text{-}PF_3)$ group is an independent illustration of the ability of such complexes to stabilize unusual ligand bonding modes.[12] We know of no fluxional processes of isocyanides analogous to eqs 3 and 4, except with the analogous MeNC complexes,[8] but terminal-bridge exchange of isocyanides is known, for example in $[Co_2(t\text{-BuNC})_8]$.[13] In $[Pt_3(\mu\text{-RNC})_3(RNC)_3]$, R = *t*-Bu, isocyanide exchange is an intermolecular process involving exchange with traces of free RNC,[13b] again very different from the mechanism of eqs 3 and 4.

Reaction with Excess Isocyanide. Complex **5** reacted slowly with excess XyNC only in the presence of sodium iodide to give the complex $[Pt_3(CNR)_4(\mu\text{-dppm})_2]^{2+}$ and free dppm (eq 5). The iodide first forms an adduct with **5**, but it has not been possible to characterize this complex or to determine the role of iodide in the overall reaction.

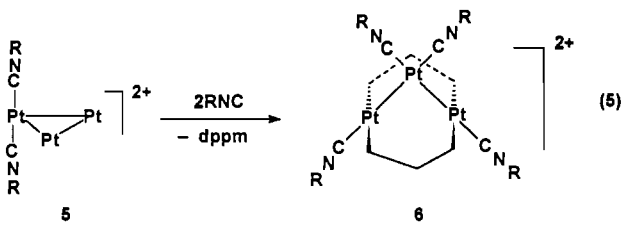

5 6 (5)

Complex **6** was characterized crystallographically and proved to be identical to the known complex, previously prepared by reaction of dppm with $[Pt_3(CNR)_8]^{2+}$ with displacement of RNC.[4c,14] Both **5** and **6** are 44-electron complexes, but whereas **5** has three Pt–Pt bonds, complex **6** has only two [nonbonding PtPt distance = 3.304(2)Å].[4c] In this sense, the bulky isocyanides are different from MeN≡C, which, when present in excess, cleaves the cluster **1** to give binuclear platinum complexes.[8] The chemistry and spectroscopic properties of the cations $[Pt_3(\mu_3\text{-CO})(CNR)(\mu\text{-dppm})_3]^{2+}$ and $[Pt_3(CNR)_2(\mu\text{-dppm})_3]^{2+}$ are otherwise similar, indicating that the preference for terminal isocyanides on platinum (compared to μ_3-CNR ligands in similar Ni_3 and Pd_3 clusters) is not a function of the steric bulk of the isocyanide ligand(s). If our interpretation of the fluxional behavior is correct, it is clear that the energy difference between the terminal and bridging isocyanide structures is small. It will be seen that an even smaller energy difference is probably present in complexes with diisocyanide ligands.

Reactions with Diisocyanides. Reaction of **1** with the diisocyanides 1,4-C≡NC_6H_4N≡C and 1,4-C≡NC_6Me_4N≡C in a 1:1 molar ratio gave complexes which are formulated as **7**,

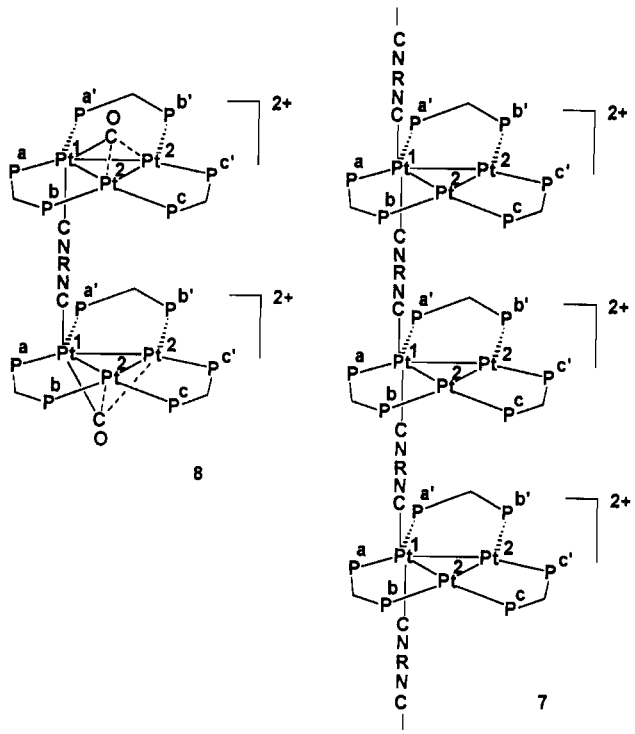

containing repeating units of Pt_3 clusters bridged by diisocyanides. The formula is supported by analytical data, and the presence of terminal isocyanides only is indicated by the observation of ν(N≡C) = 2122 and 2096 cm^{-1} for **7a,b**, respectively, with no band due to ν(CO). An interesting property of **7a** is that it gives a singlet in the ^{31}P NMR spectrum even at –80 °C, indicating that the fluxionality cannot be frozen out even at low temperature. At room temperature, the ^{31}P NMR spectrum of **7b** also gave a singlet, but this split into three broad peaks at –80 °C. The broadness is probably due partly to the oligomeric nature of the compound, but also suggests that fluxionality is also faster than in **5**. This is counterintuitive but might be explained by relatively lower steric effects when the μ-diisocyanide is bridging, thus stabilizing the transition state for fluxionality. It is noteworthy that the polymers are insoluble in nonpolar solvents and chlorinated solvents but dissolve to some extent in acetone and are easily soluble in dimethyl sulfoxide. These donor solvents may act to break down the polymeric structures to some extent and so give easier solubility. The ^{31}P NMR spectra of **7a** always gave a low-intensity singlet along with the major resonance although the compound was analytically pure. One interpretation is that this low-intensity signal may be due to the end groups in a low molar weight oligomer in solution. There has been much interest in the use of diisocyanides as bridging ligands in so-called "conjugated, rigid-rod" polymers, but these appear to be the first examples in which the diisocyanides bridge between metal cluster centers.[15]

Using only 0.5 equiv of diisocyanide, evidence was obtained for formation of complex **8**, which is analogous to the unbridged

(12) Balch, A. L.; Davis, B. J.; Olmstead, M. M. *J. Am. Chem. Soc.* **1990**, *112*, 8592.

(13) (a) Carroll, W. E.; Green, M.; Galas, A. M. R.; Murray, M.; Turney, T. W.; Welch, A. J.; Woodward, P. *J. Chem. Soc., Dalton Trans.* **1980**, 80. (b) Green, M.; Howard, J. A. K.; Murray, M.; Spencer, J. L.; Stone, F. G. A. *J. Chem. Soc., Dalton Trans.* **1977**, 1509. (c) Adams, R. D.; Cotton, F. A. In *Dynamic NMR*; Jackman, L. M., Cotton, F. A., Eds.; Academic Press: New York, 1975.

(14) The crystals of $\mathbf{6}[PF_6]_2$ were grown from aqueous methanol and were shown by Drs. Lj. Manojlovic-Muir and K. W. Muir to be both isomorphous [a = 21.508(5), b = 22.002(12), c = 18.030(12) Å; Z = 4; orthorhombic, $P2_12_12_1$] and isostructural [R = 0.066 for 1991 reflections with $I \geq 3\sigma(I)$] with those reported in ref 4c.

structure **3**. However, the complex decomposed to give **7**, **1**, and another complex which has not been identified. Also, reaction of diisocyanide with **1** at −80 °C gave complex **2d**, R = 4-C≡NC$_6$H$_4$, which is entirely analogous to the intermediates formed from simple isocyanides. As with other clusters **2**, complex **2d** decomposed on warming to give the polymer **7a** and so it was identified only by the low-temperature NMR spectra.

Discussion

Several groups have discussed structure and bonding in trinuclear clusters of platinum, and all have supported the view that single atom bridging groups, such as μ-CO, μ-RNC, or μ-SO$_2$, play an important role in stabilizing the compounds.[16] The clusters **5** were the first triplatinum clusters to be reported which did not possess such bridging groups, and so it was of interest to describe the bonding.[16] First it was important to determine if the unexpected structure might be due to steric rather than electronic factors, arising from the use of very bulky isocyanides. Hence, the corresponding complex with the less bulky MeNC was studied.[8] Since the structure is essentially the same, it is concluded that electronic factors determine the preferred structure.[8] This view is reinforced by recent observations that the isocyanide ligands bind in the triply bridging mode **D** in clusters based on the [M$_3$(μ-dppm)$_3$]$^{2+}$ cores with both M = Ni and M = Pd.[6,17] Platinum is therefore unique among the nickel group elements in preferring the terminal bonding mode **A** and, even in this case, the easy intramolecular fluxionality shows clearly that structures with bridging isocyanides are easily accessible. Extended Huckel MO calculations were carried out in order to try to rationalize the unusual structure **5**.

The MO calculations were carried out by considering the interaction of the model fragments [Pt$_3$(μ-H$_2$PCH$_2$PH$_2$)$_3$]$^{2+}$ and (HNC)$_2$. The Pt$_3$P$_6$C$_3$ atoms of the [Pt$_3$(μ-H$_2$PCH$_2$PH$_2$)$_3$]$^{2+}$ unit were assumed to be coplanar, all lying in the *xy* plane. The HNC ligands were constrained to be linear and to lie parallel to the *z*-axis and so perpendicular to the Pt$_3$P$_6$C$_3$ plane. This is the ideal orientation if the isocyanides are symmetrically triply bridging or terminal as depicted in the possible structures **E**–**H**,

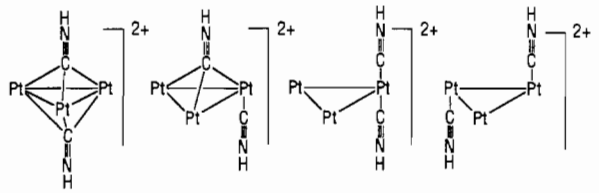

E **F** **G** **H**

as well as in symmetrical μ_2 bridging positions. Initial calculations using these idealized geometries indicated an order of stability **E** > **F** > **G** > **H** and also that structures with μ_2-HNC groups were of significantly higher energy. Calculations were carried out for both M = Pd and M = Pt, and the energy sequencies were the same in each case; they successfully predict that μ_2-HNC groups are unfavorable and that, with two terminal HNC ligands, **G** is favored over **H**. However, the EHMO calculations are not able to distinguish between the Pd and Pt cases but predict the order of stability **E** > **F** > **G** in each case. We know from experiment that **E** > **G** when M = Pd but that **G** > **E** when M = Pt. Of course, this failure is not surprising given the small energy differences involved, and a higher level of theory is clearly required to account for the quantitative aspects of the bonding. Nevertheless, valuable insights into the factors involved in determining the relative stabilities of the extreme bridging versus terminal structures **E** and **G** can be extracted, as discussed below.

A correlation diagram for both structures **E** and **G** is shown in Figure 7, and key data are shown in Figure 8. The orbitals of the [Pt$_3$(μ-H$_2$PCH$_2$PH$_2$)$_3$]$^{2+}$ fragment, represented in Figure 7 by [Pt$_3$]$^{2+}$, have been discussed previously.[16] The "cluster" orbitals are the M–M bonding orbitals e′ + a$_1$′ and the M–M antibonding orbital a$_2$′; these are hybrid orbitals and are depicted in simplified form in Figure 8a. The key role of a single atom bridging group is to stabilize the a$_1$′ MO; this is vacant in [Pt$_3$]$^{2+}$ (Figure 7) but will be occupied in clusters having the 42-electron (or higher) configuration, and so it is essential that it lie below the antibonding a$_2$′ level in stable clusters.[16] Above these cluster orbitals are the vacant orbitals a$_2$″ and e″, which have mostly platinum 6p$_z$ character and are the acceptor orbitals in Pt$_3$ clusters having >42-electron configuration.[16]

In structure **E**, which has D_{3h} symmetry, the two HNC ligands are close enough to interact; the important orbitals are the filled σ-donor orbitals of a$_1$′ and a$_2$″ symmetry and the vacant π^* acceptor orbitals of e′ and e″ symmetry (Figure 8, left side). When the fragments combine to give **E**, the orbital mixing is complex but the bonding components are still clear. The a$_1$′ donor of the (HNC)$_2$ fragment interacts with the a$_1$′ acceptor orbital of [Pt$_3$]$^{2+}$ (Figures 7 and 8a); in detail, mixing with nonbonding Pt d-levels occurs to give bonding, nonbonding, and antibonding levels (with the bonding and nonbonding levels occupied), but the net bonding arises as described above. It is this interaction which brings the cluster bonding a$_1$′ level below the antibonding a$_2$′ level (Figures 7 and 8a). The a$_2$″ donor orbital of the (HNC)$_2$ fragment overlaps with the a$_2$″ acceptor orbital derived from the empty platinum 6p$_z$ orbitals (Figures 7 and 8b). In this case there is particularly strong mixing with a filled nonbonding d$_\pi$ level (the bonding overlaps are shown in Figure 8b), and this again leads to formation of bonding, nonbonding, and antibonding levels as shown in Figure 7. The nonbonding level a$_2$″ is calculated to be the HOMO, and the cluster antibonding level a$_2$′ is the LUMO. The geometry **E** also permits back-bonding from cluster e′ orbitals to the π^* acceptor orbitals of the (HNC)$_2$ fragment; such back-bonding is calculated to be effective since the calculated charge on the (HNC)$_2$ fragment is −0.22 e.

There are some important differences in structure **G**, which has only C_{2v} symmetry. In this case, the HNC ligands are further apart and do not interact strongly; hence the fragment donor orbitals, which in C_{2v} have symmetries a$_1$ and b$_2$, are almost degenerate. As with structure **E**, d–p mixing causes added complexity, and since the lower symmetry of **G** allows more combinations, this is not shown in Figure 7. The overlap between the a$_1$ σ-donor of the (HNC)$_2$ fragment and the a$_1$ acceptor of [Pt$_3$]$^{2+}$ is weaker than in **E**, but the nonbonding level is stabilized by π-back-bonding as shown in Figure 8c. The interaction of the a$_1$ donor set with the "nonbonding" 5d$_{z^2}$ on Pt^1 is unfavorable and is illustrated schematically in Figure 8c; it is this effect which leads to a lower overall stabilization of the a$_1$ level of the [Pt$_3$]$^{2+}$ fragment and causes it to be the HOMO. The interaction of the (HNC)$_2$ fragment donor orbital of b$_2$ symmetry is localized to the 6p$_z$ acceptor orbital on Pt^1, and d–p mixing is much weaker; in this case the "nonbonding" level is therefore still in the group of closely spaced d-block levels in Figure 7. The computed HOMO–LUMO gap is smaller than for **E** (Figure 7); it is obvious that a distortion toward a bridging structure would stabilize the a$_1$ HOMO by reducing the antibonding interaction with the d$_{z^2}$ orbital on Pt^1 and so increase the HOMO–LUMO gap. Overall, the (HNC)$_2$ fragment is again a net acceptor with a computed charge of −0.1 e.

The potential energy surface between structures **E** and **G** was studied by making calculations on structures with intermediate geometry. The angle C–Pt^1–C was varied in 10° units between 180° (corresponding to structure **G**) and 81° (corresponding to structure **E**), while keeping the Pt^1–C distance at 1.97 Å. When

(15) For a summary of recent references, see: Jia, G.; Puddephatt, R. J.; Vittal, J. J.; Payne, N. C. *Organometallics* **1993**, *12*, 263.
(16) (a) Evans, D. G. *J. Organomet. Chem.* **1988**, *352*, 397. (b) Mealli, C. *J. Am. Chem. Soc.* **1985**, *107*, 2245. (c) Underwood, D. J.; Hoffman, R.; Tatsumi, K.; Nakamura, A.; Yamamoto, Y. *J. Am. Chem. Soc.* **1985**, *107*, 5968.
(17) Rashidi, M.; Kristof, E.; Vittal, J. J.; Puddephatt, R. J. *Inorg. Chem.* **1994**, *33*, 1497.

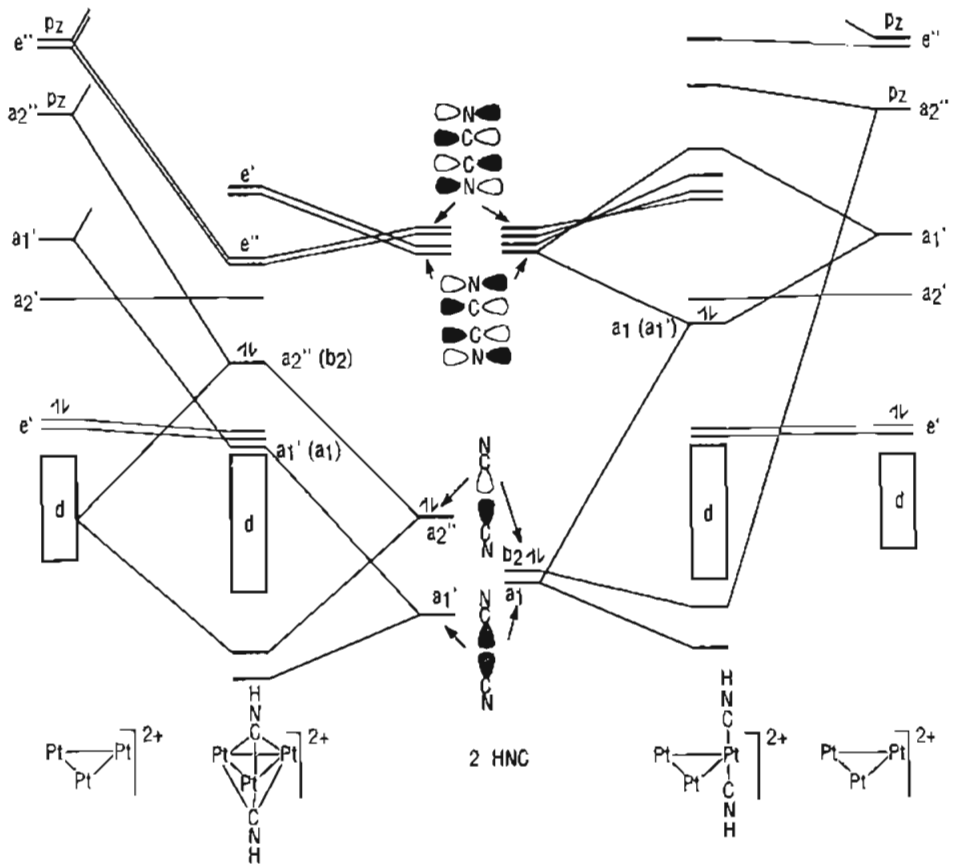

Figure 7. Energy correlation diagrams for formation of structures **E** and **G** from $[Pt_3(\mu\text{-}H_2PCH_2PH_2)_3]^{2+}$ and $(HNC)_2$. Note the different origins of the HOMO for the two structures.

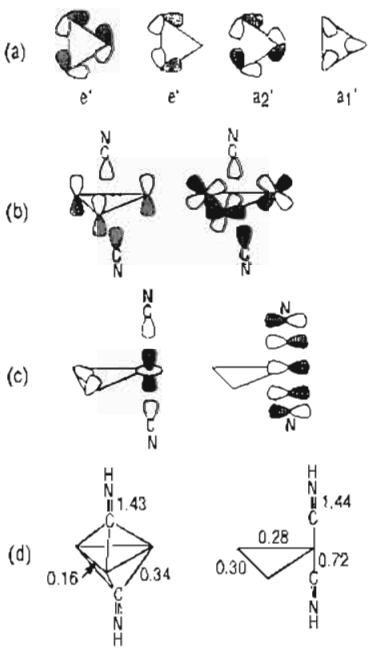

Figure 8. (a) Cluster orbitals in $[Pt_3(\mu\text{-}H_2PCH_2PH_2)_3]^{2+}$ from ref 16. (b) Two chief bonding interactions of a_2'' symmetry in **E**. For the "nonbonding" HOMO, the overlap of the ligand set with the p_z is bonding and with the d it is antibonding. (c) Two main components of the nonbonding a_1 MO for **G**. (d) Reduced overlap populations for **E** and **G**.

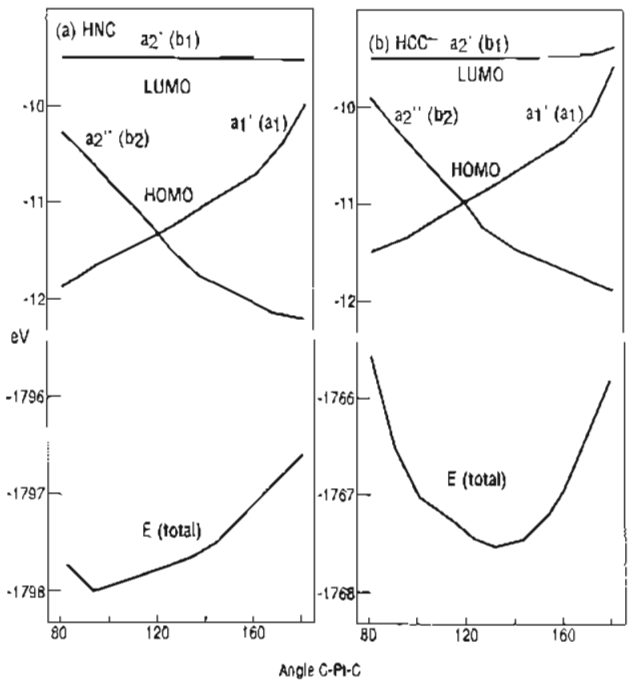

Figure 9. Energies of the LUMO and HOMO and the total energy as a function of the angle C–Pt–C in $[Pt_3(L)_2(\mu\text{-}H_2PCH_2PH_2)_3]^{2+}$ for (a) L = HNC and (b) L = HCC^-.

the angle C–Pt^1–C was reduced below 81°, the Pt^2–C and Pt^3–C distances were kept at 1.97 Å (corresponding to a shift toward the μ_2-HNC bonding mode), but the energy rose very sharply in such structures and they were not analyzed in detail. Some data from these calculations are shown in Figure 9a. It shows clearly how the character of the HOMO changes with the geometry. The symmetries are shown for the D_{3h} and, in parentheses, for the C_{2v} point groups. As the HNC ligands move from the bridging to terminal positions, the $a_2''(b_2)$ level is stabilized (because the antibonding interaction between the d-level and the $(HNC)_2$ donor is decreased as is obvious from symmetry arguments, Figure 8b), but the $a_1'(a_1)$ level is destabilized (because of the antibonding interaction between the d_{z^2} level on Pt^1 and the $(HNC)_2$ donor). It is the trade-off between these opposing effects which evidently determines the preferred geometry. The HOMO–LUMO gap

is at a maximum when the angle C–Pt^1–C is *ca.* 120°. In Figure 9a, the total energy, E(total), is shown and is at a minimum at a geometry close to structure **E** (angle C–Pt^1–C *ca.* 95°), whereas cluster **5** actually has C–Pt^1–C = 151.4(6)° approximating more closely to structure **G**. It should be noted that the model chosen disfavors intermediate structures between **E** and **G** since they will not have the perpendicular orientation of the isocyanide groups (Figures 4 and 5). We have not optimized the orientation of the HNC ligands at intermediate geometries but selected calculations indicate that this will only improve the agreement between calculated and observed structures to a minor extent. Some reduced overlap populations are given in Figure 8d. They show that the overall interaction between the $(HNC)_2$ and $[Pt_3]^{2+}$ fragments is greater for the bridged structure **E** but that the increased Pt–C bonding in **E** is balanced by lower Pt–Pt bonding compared to **G**. Note that the calculation for **G** predicts that the Pt^1–Pt^2 bond will be weaker than the Pt^2–Pt$^{2'}$ bond, in accord with the longer bond distance (Table 2). In addition, the Pt^{1}P and Pt^{2}P reduced overlap populations were 0.55 and 0.67, respectively, in accord with the longer Pt^{1}P distances (Table 2) and much lower values of ^1J(PtP) (Table 1). The somewhat lower reduced overlap population for the N≡C bonds in **E** compared to **G** (Figure 8d) is consistent with the previous conclusion that Pt–CNH back-bonding is stronger in the bridged structure. To test if this might stabilize **E**, a series of calculations was carried out using the fragments $[Pt_3]^{2+}$ and $(HC{\equiv}C^-)_2$, in which HC≡C$^-$ will be a stronger σ-donor and weaker π-acceptor than HC≡N (this is necessarily a theoretical exercise only since the reaction of HC≡C$^-$ with $[Pt_3]^{2+}$ leads to another product[18]). The results are shown in Figure 9b. The frontier orbitals are very similar to those in Figure 9a, but the potential energy surface is significantly different, with a minimum in E(total) at an angle C–Pt^1–C *ca.* 135°, clearly much closer to the terminal structure analogous to **G**. For the case of $[Pt_3]^{2+}$ with $(C{\equiv}O)_2$, the bridging structure **E** is more strongly preferred in agreement with a previous calculation;[16a] the actual structure in this case is the intermediate structure analogous to **F**.[2,11] Hence it seems that the triply bridging structure is favored for weaker σ-donor and stronger π-acceptor ligands. It has been predicted that the binding mode of CO on a Pt(111) or Pd(111) surface is similarly dependent on the relative importance of σ-donor and π-acceptor components to the bonding.[19] It is also consistent with the observation that when $[Pt_3(\mu\text{-dppm})_3]^{2+}$ units are bridged by both CO and either RNC or CN$^-$, the carbonyl is triply bridging and the RNC or CN$^-$ ligand is terminal.[20]

Overall then, these crude MO calculations do give insight into the factors which favor either the bridging structure **E** or the terminal structure **G**. They also correctly predict a soft potential energy surface in which interconversion between terminal and bridging structures should occur easily. By indicating that structures with μ_2-CNR groups lie at higher energy than either terminal or μ_3-CNR groups, they also lend credence to the proposed mechanism of fluxionality shown in eq 4.

Experimental Section

Complex **1** was prepared by the literature method.[1] The monoisocyanides were commercial samples and were used as received. The diisocyanides were prepared by the standard method and were purified by sublimation. NMR spectra were recorded by using Varian XL200 or XL300 spectrometers and were referenced to TMS (^{1}H, ^{13}C), H_3PO_4 (^{31}P), or aqueous K_2PtCl_4 (^{195}Pt, note that $\delta[PtCl_6]^{2-} = 1620$ ppm from $\delta[PtCl_4]^{2-} = 0$).[10c]

$[Pt_3(\mu_3\text{-CO})(CNC_6H_{11})(\mu\text{-dppm})_3][PF_6]_2$, 3b. $C_6H_{11}NC$ (2.2 μL) was added to complex **1** (40 mg) in acetone (10 mL). The solution was allowed to stir for 5 min, after which time the solvent was removed by reduced pressure distillation. Orange-red crystals of **3b** were isolated by crystallization from an acetone/pentane mixture in 95% yield. Anal. Calcd for $C_{83}H_{77}F_{12}NOP_8Pt_3$: C, 46.0; H, 3.6; N, 0.65. Found: C, 46.2; H, 3.6; N, 0.5. NMR at −90 °C in acetone-d_6: δ(^{1}H) = 1.2–2.6 (m, C_6H_{11}), 4.36 (m, CH_2P_2), 5.24 (m, CH_2P_2); δ(^{13}C) = 195.2 [m, ^1J(Pt^{1}C) = 1190 Hz, ^1J(Pt^{2}C) = 455 Hz, ^{13}CO]; δ(^{31}P) = −45.7 [m, ^1J(PtP^a) = 1850 Hz, ^3J(P^{a}P^c) = 170 Hz, P^a], −4.1 [m, ^1J(PtP^b) = 2550 Hz, ^3J(P^{b}P$^{b'}$) = 180 Hz, P^b], −6.7 [m, ^1J(PtP^c) = 4040 Hz, ^3J(P^{a}P^c) = 170 Hz, P^c]; δ(^{195}Pt) = −3234 (m, Pt^1), −2141 (m, Pt^2). NMR at 20 °C: δ(^{13}C) = 195 [^1J(PtC) = 688 Hz, CO]. IR (Nujol) (cm^{-1}): ν(CN) = 2170; ν(CO) = 1780. Similarly were prepared were **3a**,**c**. $[Pt_3(\mu3\text{-CO})(t\text{-BuNC})(\mu\text{-dppm})_3][PF_6]_2$, **3a**: Yield 90%. Anal. Calcd for $C_{81}H_{75}F_{12}NOP_8Pt_3$: C, 45.5; H, 3.5; N, 0.65. Found: C, 45.4; H, 3.4; N, 0.5. NMR in acetone-d_6 at −90 °C: δ(^{13}C) = 196.6 [m, ^1J(Pt^{1}C) = 1175 Hz, ^1J(Pt^{2}C) = 458 Hz, ^{13}CO]; δ(^{31}P) = −43.1 [m, ^1J(PtP^a) = 1850 Hz, ^3J(P^{a}P^c) = 170 Hz, P^a], −3.1 [m, ^1J(PtP^b) = 2510 Hz, ^3J(P^{b}P$^{b'}$) = 200 Hz, P^b], −6.7 [m, ^1J(PtP^c) = 4030 Hz, ^3J(P^{a}P^c) = 170 Hz, P^c]; δ(^{195}Pt) = −3247 (m, Pt^1); −2132 (m, Pt^2). NMR at 20 °C: δ(^{13}C) = 197 [^1J(PtC) = 685 Hz, CO]. IR (Nujol) (cm^{-1}): ν(CN) = 2165; ν(CO) = 1800. $[Pt_3(\mu3\text{-CO})(2,6\text{-Me}_2C_6H_3NC)(\mu\text{-dppm})_3][PF_6]_2$, **3c**: Yield 90%. Anal. Calcd for $C_{85}H_{75}F_{12}NOP_8Pt_3$: C, 47.4; H, 3.8; N, 0.6. Found: C, 47.5; H, 3.9; N, 0.7. NMR in acetone-d_6 at −90 °C: δ(^{1}H) = 2.70 (s, CH_3), 6.0 (br, CH_2P_2); δ(^{13}C) = 195.5 [m, ^1J(Pt^{1}C) = 1200 Hz, ^1J(Pt^{2}C) = 400 Hz, ^{13}CO]; δ(^{31}P) = −28.9 [m, ^1J(PtP^a) = 2680 Hz, ^3J(P^{a}P^c) = 160 Hz, P^a], −3.0 [m, ^1J(PtP^b) = 3200 Hz, ^3J(P^{b}P$^{b'}$) = 160 Hz, P^b], −2.8 [m, ^1J(PtP^c) = 4020 Hz, ^3J(P^{a}P^c) = 160 Hz, P^c]; δ(^{195}Pt) = −3269 (m, Pt^1); −2493 (m, Pt^2). NMR at 20 °C: δ(^{13}C) = 196 [^1J(PtC) = 685 Hz, CO]. IR (Nujol) (cm^{-1}): ν(CN) = 2131; ν(CO) = 1793.

Spectral Characterization of Intermediates, 2a,2b. Complex **1** (40 mg) was dissolved in acetone-d_6 (0.5 mL) in an NMR tube, and the solution was cooled to −78 °C. One molar equivalent of CyNC or t-BuNC was added to the cooled solution, and the samples were immediately placed in an NMR probe cooled to −92 °C. The temperature was raised by increments (between 20 and 40 °C), and the NMR spectra were monitored. The experiment was repeated with ^{13}CO labeled **1**. NMR for **2a** in acetone-d_6: δ(^{13}C) = 220.4 [m, ^1J(PtC) = 903 Hz, ^{13}CO); δ(^{31}P) = −32.5 [d, ^1J(PtP^a) = 2120 Hz, ^3J(P^{a}P^c) = 180 Hz, P^a], −55.8 [s, ^1J(PtP^b) = 3030 Hz, ^2J(PtP^b) = 410 Hz, ^3J(P^{b}P$^{b'}$) = 180, P^b], −23.4 [d, ^1J(PtP^c) = 3400 Hz, ^3J(P^{a}P^c) = 180 Hz, P^c]. NMR for **2b**: δ(^{13}C) = 217.2 [m, ^1J(PtC) = 912 Hz, ^{13}CO); δ(^{31}P) = −33.2 [d, ^1J(PtP^a) = 2220 Hz, ^3J(P^{a}P^c) = 180 Hz, P^a], −53.9 [s, ^1J(PtP^b) = 3180 Hz, ^2J(PtP^b) = 380 Hz, ^3J(P^{b}P$^{b'}$) = 180, P^b], −18.7 [d, ^1J(PtP^c) = 3240 Hz, ^3J(P^{a}P^c) = 180 Hz, P^c].

$[Pt_3(2,6\text{-Me}_2C_6H_3NC)_2(\mu\text{-dppm})_3][PF_6]_2$, 5. 2,6-$Me_2C_6H_3HC$ (2.4 mg) was added to $[Pt_3(\mu_3\text{-CO})(2,6\text{-Me}_2C_6H_3NC)(\mu\text{-dppm})_3][PF_6]_2$ (40 mg) in acetone (10 mL). The solution was stirred for 10 min at room temperature, after which time the solvent was removed by reduced pressure distillation. Dark red crystals of complex **5** were isolated by crystallization from an acetone/pentane mixture. Anal. Calcd for $C_{96}H_{90}F_{12}N_2P_8$: C, 49.1; H, 3.5; N, 1.2. Found: C, 49.3; H, 3.7; N, 1.2. IR: ν(CNR) = 2122 cm^{-1}. NMR in acetone-d_6: δ(^{1}H) = 2.30 (s, CH_3); 5.82 (br, P_2CH_2); δ(^{31}P) −41.4 [d, ^1J(PtP^a) = 1760 Hz, ^3J(P^{a}P^c) = 160 Hz, P^a], −1.3 [s, ^1J(PtP^b) = 2440 Hz, ^3J(P^{b}P$^{b'}$) = 220, P^b], −10.7 [d, ^1J(PtP^c) = 4030 Hz, ^3J(P^{a}P^c) = 160 Hz, P^c]; δ(^{195}Pt) = −3190 [m, ^1J(Pt^{1}Pt^2) = 900, Pt^1], −2002 [m, ^1J(Pt^{1}Pt^2) = 900 Hz, Pt^2], J(PtP) couplings as reported in ^{31}P NMR data.

Detection of Intermediate Complex 4. $[Pt_3(\mu_3\text{-CO})(2,6\text{-Me}_2C_6H_3NC)(\mu\text{-dppm})_3][PF_6]_2$ (40 mg) was dissolved in acetone-d_6 (0.5 mL). The solution was transferred to an NMR tube, and the tube and its contents were cooled to −78 °C. 2,6-$Me_2C_6H_3NC$ (2.4 mg) was added to the NMR tube, which was then placed in the probe of the NMR spectrometer which had been previously cooled to −92 °C. The ^{31}P{^{1}H} NMR spectra of the reaction species were monitored by raising the temperature in 40° increments up to 20 °C. The experiment was repeated with ^{13}CO labeled **1**. NMR: δ(^{13}C) = 217.4 [m, ^1J(PtC) = 908 Hz, ^{13}CO); δ(^{31}P) = −34.8 [d, ^1J(PtP^a) = 2200 Hz, ^3J(P^{a}P^c) = 200 Hz, P^a], −56.5 [s, ^1J(PtP^b) = 3090 Hz, ^2J(PtP^b) = 348 Hz, ^3J(P^{b}P$^{b'}$) = 180 Hz, P^b]; −17.7 [d, ^1J(PtP^c) = 3380 Hz, ^3J(P^{a}P^c) = 200 Hz, P^c].

$\{[Pt_3(\mu\text{-1,4-C}{\equiv}NC_6H_4N{\equiv}C)(\mu\text{-dppm})_3][PF_6]_2\}_n$, 7a. To a stirred solution of **1** (40 mg) in CH_2Cl_2 (2 mL) was added dropwise a solution of 1,4-CNC_6H_4NC (2.5 mg) in CH_2Cl_2 (1 mL). A red solid slowly precipitated. After 16 h, the red product was separated by filtration, washed with CH_2Cl_2 (1 mL), and dried under vacuum: Yield 70%; mp 300–305 °C. Anal. Calcd for $C_{83}H_{70}F_{12}N_2P_8Pt_3$: C, 46.2; H, 3.2; N, 1.3. Found: C, 46.3; H, 3.8; N, 1.1. NMR in acetone-d_6: δ(^{31}P) = −14.5 [s, ^1J(PtP) = 3030 Hz, dppm]; −15.45 [s, ^1J(PtP) = 3000 Hz, dppm]; relative intensities 5:1. NMR in dmso-d_6: δ(^{31}P) = −15.7 [s,

(18) Jennings, M. C.; Manojlovic-Muir, Lj.; Puddephatt, R. J. *J. Am. Chem. Soc.* **1989**, *111*, 745.
(19) Anderson, A. B.; Awad, M. K. *J. Am. Chem. Soc.* **1985**, *107*, 7854.
(20) Jennings, M. C.; Puddephatt, R. J.; Manojlovic-Muir, Lj.; Muir, K. W.; Mwariri, B. N. *Inorg. Chim. Acta* **1993**, *212*, 191.

Table 3. Crystallographic Data for $[Pt_3dppm_3\{CNC_6H_3(CH_3)_2\}_2]\cdot 0.5C_3H_6O,C_5H_{12}$, **5**

$C_{97}H_{93}F_{12}N_2O_{0.50}P_8Pt_3$	fw = 2355.76
a = 17.639(2) Å	space group $P2_1$ (No. 4)
b = 19.704(3) Å	T = 22(2) °C
c = 14.5444(12) Å	λ = 0.710 73 Å
β = 101.99(2)°	μ = 44.30 cm^{-1}
ρ(obsd) = 1.65(2) g·cm^{-3}	ρ(calcd) = 1.582 g·cm^{-3}
V = 4944.7(12) Å^3	Z = 2
$R(F_o)^a$ = 0.0393	$R_2(F_o^2)^a$ = 0.0940

^{a} $R = \sum(||F_o| - |F_c||)/\sum|F_o|$; $R_2 = [\{\sum w(|F_o^2| - |F_c^2|)^2\}/\sum w(F_o^2)^2]^{0.5}$.

^1J(PtP) = 3048 Hz, dppm]; –16.6 [s, ^1J(PtP) = 3000 Hz, dppm], relative intensities 5:1. IR (Nujol) (cm^{-1}): ν(N≡C) = 2122 (s); ν(CO) absent.

Similarly was prepared $\{[Pt_3(\mu\text{-}1,4\text{-}C{\equiv}NC_6Me_4N{\equiv}C)(\mu\text{-dppm})_3][PF_6]_2\}_n$, **7b**: Yield 75%; mp 266–269 °C. Anal. Calcd for $C_{87}H_{78}F_{12}N_2P_8Pt_3$: C, 47.2; H, 3.5; N, 1.3. Found: C, 47.2; H, 3.6; N, 1.3. NMR in acetone-d_6: $\delta(^{31}P)$ at 20 °C = –15.2 [s, ^1J(PtP) = 3150 Hz, dppm]; $\delta(^{31}P)$ at –80 °C = –10, –14, –25 (each broad multiplet, dppm). IR (Nujol) (cm^{-1}): ν(N≡C) = 2096 (s).

$Pt_3(\mu\text{-CO})(\eta^1\text{-}1,4\text{-}CNC_6H_4NC)(\mu\text{-dppm})_3[PF_6]_2$, 2d. To a solution of **1** (30 mg) in CD_2Cl_2 (0.3 mL) in an NMR tube cooled to –78 °C was added a solution of 1,4-CNC_6H_4NC (2 mg) in CD_2Cl_2 (0.2 mL), and the tube was transferred to the NMR probe which was precooled to –80 °C. The product was characterized by its NMR spectrum at –80 °C. NMR in CD_2Cl_2: $\delta(^{31}P)$ = –14.9 [d, $^1J(P^aPt^1)$ = 3372 Hz, $^3J(P^aP^c)$ = 191 Hz, $2P^a$], –47.15 [s, $^1J(P^bPt^2)$ = 3300 Hz, $^2J(P^{b'}Pt^2)$ = 480 Hz, $^3J(P^bP^{b'})$ = 180 Hz, $2P^b$], –37.45 [d, $^1J(P^cPt^2)$ = 2200 Hz, $^2J(P^cPt^1)$ = 270 Hz, $^3J(P^cP^a)$ = 191 Hz, $2P^c$].

$[\{Pt_3(\mu\text{-CO})(\mu\text{-dppm})_3\}_2(\mu\text{-}1,4\text{-}CNC_6H_4NC)][PF_6]_4$. To a stirred solution of **1** (50 mg) in CH_2Cl_2 (40 mL) was added a solution of 1,4-CNC_6H_4-NC (1.6 mg) in CH_2Cl_2 (40 mL). The solution became darker red in color. After 1 h, the solvent was evaporated to give the impure product as a red solid. The ^{13}CO labeled complex was prepared in a similar way. NMR in CD_2Cl_2: $\delta(^{31}P)$ = –5.0 [s, broad, ^1J(PtP) = 3760, dppm]; $\delta(^{195}Pt)$ = –2560 [v br, Pt]; $\delta(^{13}C)$ = 205 [m, ^1J(PtC) = 800 Hz, ^{13}CO]. IR (Nujol) (cm^{-1}): ν(C≡N) 2125; ν(CO) = 1733. On attempted recrystallization, the complex decomposed to give the polymer **7a** and some **1**.

$[Pt_3(2,6\text{-}Me_2C_6H_3NC)(\mu\text{-}1,4\text{-}CNC_6Me_4NC)(\mu\text{-dppm})_3][PF_6]_2$. To a solution of **3c** (40 mg) in acetone (10 mL) was added a solution of 1,4-CNC_6Me_4NC (3.4 mg) in acetone (5 mL). After 10 min, the volume was reduced to 4 mL and hexane (10 mL) was added to precipitate the product as an impure red powder. NMR at –80 °C in acetone-d^6: $\delta(^{31}P)$ = –41.4 [d, ^1J(PtP) = 1740 Hz, $^3J(P^aP^c)$ = 161 Hz, $^2J(PtP^a)$ = 300 Hz, P^a], –1.2 [s, ^1J(PtP) = 2400 Hz, $^3J(P^bP^{b'})$ = 200 Hz, P^b], –8.2 [d, ^1J(PtP) = 4160 Hz, $^3J(P^aP^c)$ = 161 Hz, P^c]. IR (Nujol) (cm^{-1}): ν(CN) = 2102. The NMR also indicated the presence of **5** and **7b**, and these could not be separated by recrystallization.

X-ray Structure Determination. Data Collection and Reduction. Red, efflorescent crystals with equant habit of $[Pt_3(\mu\text{-dppm})_3\{C{\equiv}NC_6H_3(CH_3)_2\}_2][PF_6]_2$, **5**, were grown from acetone/*n*-pentane solutions at room temperature. ^1H NMR spectroscopy of the sample from which crystals were picked for the structure determination indicated the presence of acetone and *n*-pentane in the crystal lattice. Crystals and mother liquor were sealed in Lindemann capillaries for the X-ray studies.

A preliminary photographic examination showed Laue symmetry $2/m$, and the systematic absences observed determined the space group as $P2_1$ or $P2_1/m$. The crystal density was determined by neutral buoyancy, and with two formula units per cell, site symmetry m or $\bar{1}$ is imposed upon the cation in $P2_1/m$.[21] Crystal data for **5** are given in Table 3.

The structure was determined from data collected on an Enraf-Nonius CAD4F diffractometer. Cell constants and an orientation matrix were refined using the angular settings for carefully centered, high-angle reflections.[22] ω-Scans of intense, low-angle reflections indicated a satisfactory crystal quality. Intensity data were recorded at variable scan speeds within a maximum time per datum of 75 s. Background estimates were made by extending the scan by 25% on each side.[22] Standard reflections were monitored regularly and showed only random variations of less than 1%. The data were processed using the Enraf-Nonius Structure Determination Package, Version 3.0,[23] running on a PDP 11/23+ computer. Standard deviations were assigned on the basis of counting statistics, and an empirical absorption correction was applied.[24] An $N(Z)$ test[25] on the 8456 data did not distinguish between the centric and noncentric space groups.

Structure Solution and Refinement. Since m symmetry for the cation is possible, a solution was first attempted in space group $P2_1/m$ but with no success. The structure was solved readily by Patterson and Fourier techniques in space group $P2_1$. Symmetry-equivalent forms were averaged to yield 8174 data for solution and refinement of the structure, and preliminary refinement was by full-matrix least-squares techniques on F.[23] However, the presence of disordered PF_6 anions, and sites partially occupied by acetone and *n*-pentane solvent molecules, complicated the refinement. A satisfactory completion of the analysis was finally achieved using the soft restraints available in SHELXL-93.[26] In the final model, the twelve phenyl rings and the two xylyl groups were defined as residues with 2-fold symmetry using soft restraints. The remaining atoms in the cation were assigned anisotropic thermal parameters. Each of the two PF_6 anions showed two orientations in the lattice; a disorder model consisting of rigid groups [P–F = 1.57 Å; multiplicities 50:50 for P(7) and P(7′) and 60:40 for P(8) and P(8′), respectively] satisfactorily accounted for the electron density. The acetone and pentane sites were partially occupied, and atom multiplicities of 0.5 gave reasonable thermal parameters. The acetone molecule was refined as a rigid group, while soft restraints were placed upon the pentane geometry. A difference Fourier synthesis showed clear evidence for most of the H atoms, so all were included using a riding model. A total of 22 data with strongly negative intensities were dropped. In the final calculations, all atoms were included and an extinction coefficient was refined. The Flack absolute structure parameter refined to –0.010(10), indicating that the hand of the model matched that of the crystal.[27] A total difference Fourier synthesis showed no peaks of any chemical significance, and an analysis of variance showed no unusual trends. A summary of the refinement is given in Table 3.

Table S1, anion, solvent, and hydrogen atom positional and thermal parameters, Table S2, anisotropic thermal parameters, Table S3, a plane, Table S4, full bond lengths and bond angles, and Table S5, crystal data and experimental details, have been deposited.

EHMO Calculations. Averaged bond distances and angles from X-ray structures of **5** and related molecules were taken, including Pt–Pt = 2.63 Å, Pt–P = 2.32 Å, Pt–C = 1.97 Å, C≡N = 1.19 Å, P–Pt–P = 109°, P–Pt–Pt = 95°, and H–N–C = 180°. EHMO parameters and methodology were taken from ref 28.

Acknowledgment. We thank the NSERC (Canada) for financial support, Dr. T. Marder for valuable discussions, and Shiraz University, Shiraz, Iran, for granting a sabbatical leave to M.R.

Supplementary Material Available: Tables of anion, solvent, and hydrogen atom positional and thermal parameters, anisotropic thermal parameters, a least-squares plane, full bond lengths and angles, and crystal data have been deposited (10 pages). Ordering information is given on any current masthead page. Structure amplitude tables are available from the authors.

(21) *International Tables for X-ray Crystallography*; D. Reidel Publishing Co.: Boston, MA, 1983; Vol. A.

(22) Enraf-Nonius CAD4 Operators Manual, Enraf-Nonius Delft, Delft, The Netherlands, Version 5.0, 1984.

(23) Enraf-Nonius Structure Determination Package, SDP-Plus, Version 3.0, 1985.

(24) North, A. C. T.; Phillips, D. C.; Mathews, F. S. *Acta Crystallogr.* **1968**, *A24*, 351.

(25) Howells, E. R.; Phillips, D. C.; Rogers, D. *Acta Crystallogr.* **1950**, *3*, 210.

(26) Sheldrick, G. M. SHELXL-93. *J. Appl. Crystallogr.* **1993**.

(27) Flack, H. D. *Acta Crystallogr.* **1983**, *A39*, 876.

(28) (a) Summerville, R. H.; Hoffmann, R. *J. Am. Chem. Soc.* **1976**, *98*, 7240. (b) Rossi, A.; Howell, J.; Wallace, D.; Haraki, K.; Hoffmann, R. Program ICON8, QCPE No. 517. *QCPE* **1986**, *6*, 100.